Biol Cybern (2013) 107:513–527
DOI 10.1007/s00422-013-0566-2

ORIGINAL PAPER

Biological Cybernetics

A bioinspired autonomous swimming robot as a tool for studying goal-directed locomotion

L. Manfredi · T. Assaf · S. Mintchev · S. Marrazza · L. Capantini · S. Orofino · L. Ascari · S. Grillner · P. Wallén · Ö. Ekeberg · C. Stefanini · P. Dario

Received: 23 March 2012 / Accepted: 13 August 2013 / Published online: 13 September 2013

Abstract The bioinspired approach has been key in combining the disciplines of robotics with neuroscience in an effective and promising fashion. Indeed, certain aspects in the field of neuroscience, such as goal-directed locomotion and behaviour selection, can be validated through robotic artefacts. In particular, swimming is a functionally important behaviour where neuromuscular structures, neural control architecture and operation can be replicated artificially following models from biology and neuroscience. In this article, we present a biomimetic system inspired by the lamprey, an early vertebrate that locomotes using anguilliform swimming. The artefact possesses extra- and proprioceptive sensory receptors, muscle-like actuation, distributed embedded control and a vision system. Experiments on optimised swimming and on goal-directed locomotion are reported, as well as the assessment of the performance of the system, which shows high energy efficiency and adaptive behaviour. While the focus is on providing a robotic platform for testing biological models, the reported system can also be of major relevance for the development of engineering system applications.

Keywords Bioinspired autonomous robot · Lamprey-like robot · Goal-directed locomotion · Muscle-like actuation · Compliant robot · Distributed control

L. Manfredi, T. Assaf, L. Capantini and L. Ascari were formerly at SSSA.

This article forms part of a special issue of *Biological Cybernetics* entitled “Lamprey, Salamander Robots and Central Nervous System”.

L. Manfredi
Institute for Medical Science and Technology (IMSaT), University of Dundee, Wilson House, 1 Wurzburg Loan, Dundee Medipark, Dundee DD2 1FD, UK
e-mail: mail@luigimanfredi.com

T. Assaf
Bristol Robotics Laboratory, Frenchay Campus, Bristol BS16 1QY, UK

S. Mintchev · S. Marrazza · S. Orofino · C. Stefanini (✉) · P. Dario
The BioRobotics Institute, Scuola Superiore Sant’Anna (SSSA), Viale Rinaldo Piaggio 34, 56025 Pontedera (Pisa), Italy
e-mail: c.stefanini@sssup.it

L. Capantini · S. Grillner · P. Wallén
Department of Neuroscience, Nobel Institute for Neurophysiology, Karolinska Institutet (KI), Retziusväg 8, 171 77 Stockholm, Sweden

L. Ascari
HENESIS srl, Viale dei Mille 108, 43125 Parma, Italy

Ö. Ekeberg
Department of Computational Biology, School of Computer Science and Communication, Royal Institute of Technology, Kungliga Tekniska Högskolan (KTH), 100 44 Stockholm, Sweden

1 Introduction

Experiments on animals have, for a long time, been the only viable approach in order to validate theories and hypotheses in neuroscience. For instance, this applies to the mechanisms underlying goal-directed locomotion in living organisms. Animal experiments enable validation of organism-level theories; however, they are often difficult to perform due to a variety of ethical and methodological factors. Consequently, conducting tailored experiments on animals focusing on goal-directed locomotion requires great effort.

Progress in the technology of robotics has opened up new opportunities for applications in biological research. Robotics enable the use of advanced machines, capable of perceiving the environment and acting within it. Historically, robot design has often been inspired by living organisms in order to develop systems with better reactive behaviour in the real world (Beer et al. 1997). The adoption of bioinspired approaches in robot design has led to advancement in engineering technology, especially in terms of more compliant and reliable mechanisms, and new developments in materials, sensors, actuators, control schemes and energy efficiency (Hochhalter 2011; Barranco et al. 2009; Hu et al. 2010; Mazzolai et al. 2011; Durr et al. 2004; Scarfogliero et al. 2009).

Bioinspired robots have become a useful scientific tool for studying biological systems (Kawato 2000; Manfredi et al. 2006, 2009; Ascari et al. 2009; Chiel et al. 2009) and in particular various animal forms (Webb 2001; Webb and Consi 2001; Stefanini et al. 2012; Li et al. 2012). These developments have brought about a new methodological approach to the study of biological systems.

This new methodology consists of adopting neurobiological knowledge and models directly in artefacts that are capable of autonomous behaviour in the physical world. Neuroscientists and computational neurobiologists can "program" jointly with roboticists, by designing the machinery of these artefacts in order to observe the resulting behaviour when interacting with the physical world.

Recent research has reported cases where robots were able to replicate the neurological systems, which have been seen as a valid hypothesis within the field of neuroscience.

Webb reported on the process of biological model validation using a robot (Webb 2008). Earlier (Webb 2000), this author proposed a discussion on the topic "What does robotics offer animal behaviours?", which is the inverse of "What does animal behaviour offer robotics?" reported by Arkin (1998, p. 52). In this work, Webb presented a wide description of how robot-based research can become a new approach to investigate animal behaviour. She gave an objective description of the robot-validation approach compared to a simulation approach. In a later paper (Webb 2001), the same author proposed a new discussion on the validation of biological models with robots. In this work the author proposed a detailed description of the process needed to build a simulation in order to demonstrate behaviours of biological models. Differing from the former work, the author gave more detail about the interpretation of the results, which came from the validation. Kawato (2000) has reviewed the current understanding of brain mechanisms by using robots. In a more recent review, Ijspeert describes the use of central pattern generators (CPGs) in biology and in robotics (Ijspeert 2008). The outcomes for neurobiology given by this new class of experimental tools are evident: models can be implemented in bioinspired robots, and the resulting behaviours can be observed, thus helping in the attribution of behaviours to specific neural mechanisms. However, some constraints in the actual technologies could act as a limitation to the understanding of the biological model. These limitations provide reciprocal feedback and a stimulus to engineers to redesign and improve the current technology in terms of mechanics, sensors and new strategies of control able to adapt and to operate in unstructured environments (Bar-Cohen 2012).

This paper presents a bioinspired autonomous swimming robot as a tool for neuroscientists to study goal-directed locomotion control and related neural control mechanisms, adopted from the lamprey model aimed at vertebrate locomotion. The robotic artefact mechanics were inspired by the real animal structure mimicking the flexibility and the passive dynamic movement utilising custom-designed actuators. The electronic digital control is distributed along the body in order to replicate the distributed architecture of CPGs in the animal spinal cord. A stereo vision system is included which can implement models of visuo-coordination for goal-directed locomotion. Both the mechanical and the electronic design have high energy efficiency, allowing the robot to continuously perform up to 5 h. Experimental results, presented in the article, prove a satisfactory level of biomimesis and open the way to a number of future investigations, as discussed in the final section.

2 Locomotor control system in lamprey: a general description

The ability of moving and orienting in the environment is undoubtedly of crucial importance for all living animals, from the invertebrates to the vertebrates. Even the basic motor task of locomotion requires the coordinated activity of a set of neural control systems providing propulsion, equilibrium/stability, steering and adaptation to the environment. Neural circuits located within the spinal cord accomplish the pattern-generating function of locomotor control (i.e. the sequential activation and precise timing of appropriate muscles). These neural circuits are usually referred to as central pattern generators (CPGs) (Grillner 2003), and they control the activity of spinal motor neurons and, hence, force production in the muscles. The control systems appear very similar among all vertebrates, from lamprey to mammals, and they are to a large extent conserved throughout vertebrate evolution, although the locomotor movements themselves differ between types of locomotion (e.g. walking, swimming, flying) but also between species, where each species can display specific characteristics (Grillner and Jessell 2009). The preservation of the control system for locomotion implies that in all vertebrates the same principles to control movement coordination are governed by similar functional units. In this scenario, the lamprey, one of the first vertebrates to emerge about 560 million years ago (Rovainen 1979), has become a prototype for the studies on vertebrate locomotion. The lamprey is an experimentally amenable model to study from the cellular/molecular level up to the behavioural

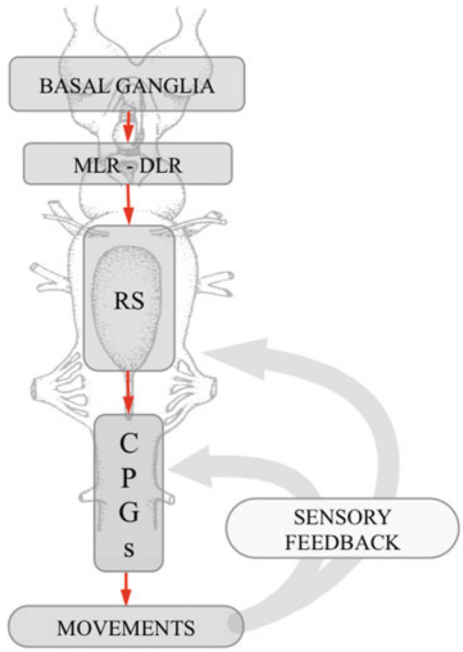

Fig. 1 Main subsystems involved in the control of motor behaviour

level due to the relative simplicity of the neuronal structures of its locomotor control system.

Figure 1 illustrates the general organisation of the locomotor control system. In all vertebrates, the interconnected CPG networks within the spinal cord generate the species-specific locomotor movements involved in the control of locomotion and are responsible for the sequential activation of the different muscle groups. The CPG networks also receive movement-related feedback involved in the adaptation and correction of any perturbation occurring during each phase of locomotion. The CPG networks are turned on from evolutionarily conserved brainstem locomotor command areas (mesencephalic and diencephalic locomotor regions—MLR and DLR) that, through the reticulospinal system (RS), a group of excitatory neurons located along the brainstem, provide excitation to the spinal circuits. The activation of the RS system results in the transition between the quiescent and the active behavioural state in the animal. These components constitute the propulsive neural machinery, where the underlying operational mechanisms were elucidated for the lamprey model system (Grillner 2003; Grillner and Graybiel 2006; Grillner et al. 2007).

Another relevant system involved in the goal-directed locomotor is visuo-motor coordination, which plays an important role in this behaviour. A specific research objective is to further investigate the physiological processes underlying visuo-motor coordination in lamprey through biological experiments in combination with computer simulations and robotic system validations.

The locomotor command areas in the brainstem and the CPG systems were replicated on the artefact presented in this work. The basic mechanisms of functioning have been modelled and implemented on board and described in more detail in the following sections.

3 The biorobotic lamprey

The interaction between the central pattern generators and the generated swimming movements in the lamprey has previously been studied in simulations (Ekeberg 1993; Ekeberg and Grillner 1999). Several swimming robotic platforms have been implemented to investigate swimming locomotion behaviour. Hirose has compiled a tutorial on a snake-like robot, where he presents his previous amphibious artefact named ACM-R5 (Hirose and Yamada 2009). Ayers et al. (2000) presented an autonomous lamprey robot, which used shape memory alloy (SMA) as actuators. Crespi and Ijspeert (2009) reported on a robotic salamander used to validate the amphibious behaviour of the CPG.

This section describes the autonomous robotic lamprey, which was designed in order to replicate a simplified model of the living animal. The robot, one metre long, is composed of ten active segments (mimics of myotomes), and the design of the mechanical structure allows the robot to achieve compliant movements. The actuators are laid out in a symmetric left/right antagonistic configuration, and on-board proprioceptive sensors measure the curvature of the robot in order to replicate the function of stretch receptors in the animal. The tail allows the robot to improve the swimming performance. A distributed digital control replicates the CPG, and two miniaturised cameras implement the stereo vision system.

The components of the bioinspired system and their corresponding subsystems in the real animal are shown in Fig. 2.

3.1 The mechanical design

Anguilliform swimming, which is used by the lamprey, arises from the interaction between water and body deformation. The artificial replication of such swimming therefore requires a structure that is deformable, ideally continuously deformable, and controlled by means of force-controlled and compliant muscle-like actuators (Madden et al. 2004). It is well understood that artificial mechanical and natural biological (muscle) actuator systems have very different physical properties and that the design and control of adaptive motor systems is still a persistent and fundamental challenge in biomimetic robotics. The design of the presented lamprey robot has sought solutions to avoid some of the most limiting mechanical constraints, and a novel actuator system based on permanent magnets has been conceived by the authors. It is controlled by a simulated central pattern generator emulating the lamprey's natural motor command chain. The design of the aforementioned actuator is based on two novel con-

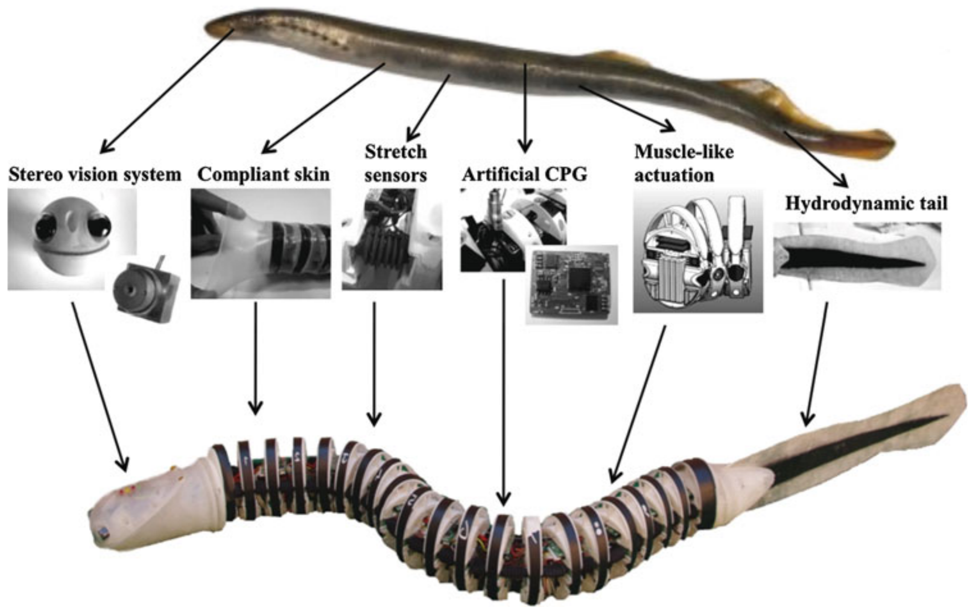

Fig. 2 The model and the artefact. This scheme describes the similarities between the animal and the presented artefact. The robot is composed of a stereo vision system, stretch sensors receptor, distributed control, hydrodynamic tail and a compliant waterproof silicone skin

cepts: the use of the direct interaction between permanent magnets to generate actuation forces and the control of actuation forces by acting on the relative orientation or position of the magnets by using dedicated servomotors.

The actuators developed according to these working principles can generate force-driven, compliant and efficient movements mimicking the behaviour of natural muscles. Furthermore, permanent magnets can transmit forces without any mechanical connection improving energy efficiency and simplifying the overall design of the actuator and its integration with the robot body.

The working principle of a generic permanent magnet actuator is reported in Fig. 3 considering two magnets: one connected to a rotational joint while the other one can only translate. This magnetic layout has an equilibrium position shown in Fig. 3a where the right magnet can freely translate without being subject to any force. The maximum achievable attractive or repulsive forces are obtained respectively with a 90° rotation of the circular magnet in either clockwise or counterclockwise directions (Fig. 3c, b). Intermediate rotations generate force levels from zero to maximum attraction or repulsion values.

The aforementioned actuator was conceived in order to overcome the limitations of conventional actuators (e.g. electromagnetic motors commonly used in robotics), which have performances and properties different from those achieved by the natural muscles (Hunter and Lafontaine 1992). Although electromagnetic actuators have a power-to-mass ratio significantly superior to natural muscles, their mechanical power is mainly available at high speed with lower forces compared to those that can be generated by muscular tissue. Torque density can be tuned by adding reduction gears; however, this increases the passive impedance of the actuators due to additional inertias, irreversibility, friction, reduction in compliance and poor stiffening capabilities. In order to preserve high torque density without compromising the impedance, two approaches are commonly used. The first consists of modulating the apparent impedance of the actuator by using dedicated control algorithms and by employing torque and full status feedback (Albu-Schaffer et al. 2007; Ott et al. 2008). Although this technique was demonstrated to be successful in many applications, these control algorithms are an artificial expedient that is not appropriate for robots being conceived as tools for neuroscientific model validation. Being interested in highly adaptive systems, the artefact behaviour cannot be pre-programmed (Pfeifer et al. 2005); on the contrary, locomotion will emerge from the exploitation of intrinsic material properties of the agent, and the interaction between the artefact and the environment. In this way, behaviour will be not only internally generated, but it will result from a system–environment interaction. This implies that much attention has to be paid in making this interaction as close as possible to the one shown by the living animal.

The second approach involves the use of an additional compliant element—e.g. a spring (Pratt and Williamson 1995)—together with a servomotor (electromagnetic actuator coupled with reduction gears). This solution has intrinsic mechanical impedance that can be tuned according to the stiffness of the elastic elements. Additionally, the primary output of the actuator (servomotor coupled with a compliant element) is a force that can be controlled according to the deformation of the compliant element. For these reasons, we can assume that this system is force-driven and compliant, similar to natural muscles. A robotic system with a stiff servomotor (high mechanical impedance) has its shape governed by actuators. On the other hand, if adopting an intrin-

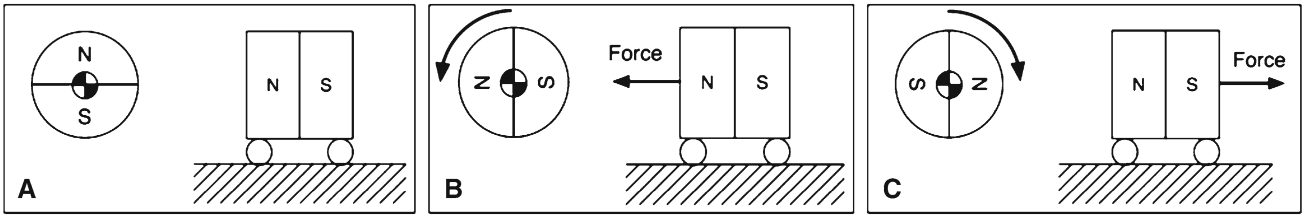

Fig. 3 Working principle of the actuator. The force is generated by the interaction between two magnets. By modifying the orientation of the circular magnet, the direction and the intensity of the actuation force are controlled. Three different orientations of the circular magnet correspond to: **a** zero force (neutral configuration), **b** attraction force and **c** repulsive force

sically compliant and force-driven actuator (low mechanical impedance), the locomotion and the posture of the robot result not only from actuation stimuli but also from the external forces exchanged with the environment. This phenomenon is due to the intrinsic compliance of both the actuator and the body of the artefact.

Pratt and Williamson (1995) proposed a compliant actuator, which relies on springs coupled with servomotors instead of using permanent magnets. The major difference between the aforementioned and the proposed actuator is the use of permanent magnets instead of springs. Unlike spring actuators, permanent magnets can transmit forces without contact, simplifying the design and improving the efficiency of the robot.

Figure 4 describes a 3D model of the vertebrae and the working principle of the new kind of muscle-like actuation system designed by using direct magnet interaction for producing forces (Stefanini et al. 2011) instead of using springs.

The presented robot has a modular design based on ten independent and flexible segments comprised of a middle active vertebra (V2), which is magnetically coupled with two passive ones (V1 and V3). The flexible segment has a total length of 61.6 mm and a minimum curvature radius of 48 mm. The active vertebrae (Fig. 4a) are equipped with a servomotor (c) to control the orientation of a shaft, on which two cylindrical magnets with radial magnetisation (a.1 and a.2) are placed (one for each side of the vertebra). The two magnets are axially aligned, but their orientation is opposite (i.e. they are axially aligned with opposing polarity, with a 180° rotation). The passive vertebrae (Fig. 4b) are equipped with two fixed magnets (h.1 and h.2), one for each side and with the same orientation. Furthermore, each passive vertebra contains a battery pack (j) and control electronic boards (k), which are described in more detail in the section "control electronic boards". In order to mimic a flexible notochord, the vertebrae are connected together with two wires (e.1, e.2, e.3 and e.4) made of spring steel.

The novel actuator is based on direct permanent magnet interaction to generate actuation forces that can be controlled by servomotors acting on the relative orientation of magnets. This operating principle is described in Fig. 4c, d: when the

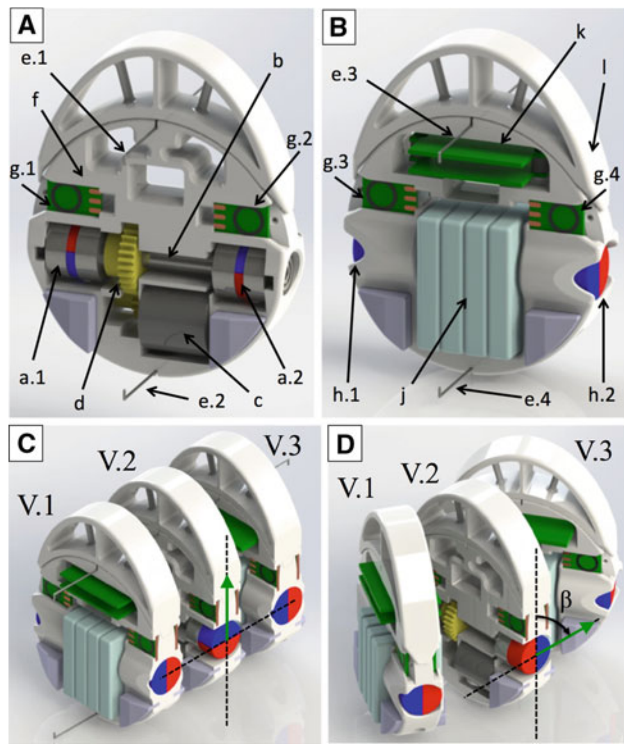

Fig. 4 Design of the vertebrae and working principle of the magnetic actuator. **a** describes the design of the active vertebrae: *a* movable cylindrical magnets, *b* shaft, *c* servomotor, *d* gears, *e* notochord, *f* frame, *g* boards to connect the stretch sensors. **b** describes the design of the passive vertebrae: *h* fixed cylindrical magnets, *e* notochord, *j* batteries, *k* electronic boards, *l* frame, *g* electronic boards to connect stretch sensors signals. **c** and **d** describe the working principle of the permanent magnet actuator developed for the lamprey robot. In both pictures, a cross section shows the layout of the permanent magnets. **c** is the neutral configuration where the bending moment of the magnets is zero. By rotating the magnets inside the active vertebra of −90°, the magnets on the right side repel each other, while the magnets on the left side are attracted generating the left bending of the segment

orientation of the active magnets (a.1 and a.2) is perpendicular to one of the fixed magnets (h.1 and h.2), a neutral configuration is achieved ($\beta = 0°$). In this layout, the value of the bending moment is zero; thus, the vertebrae are parallel, and the segment is straight (Fig. 4c). The servomotor can modify the orientation of the magnets (max rotation of ±90°),

Fig. 5 Performance of the magnetic actuator. **a** reports the torque required by the servomotors to modify the orientation (β angle) of the two active magnets when the vertebrae are parallel (T_p) or in the maximum bend configuration (T_b). **b** reports the bending moments of the permanent magnets and the elastic notochord in relation to the radius of curvature of the segment. M_n and M_a refer respectively to the condition when the vertebrae are in the neutral and in the maximum attraction configuration. $-M_e$ refers to elastic bending moment generated by the elastic notochord

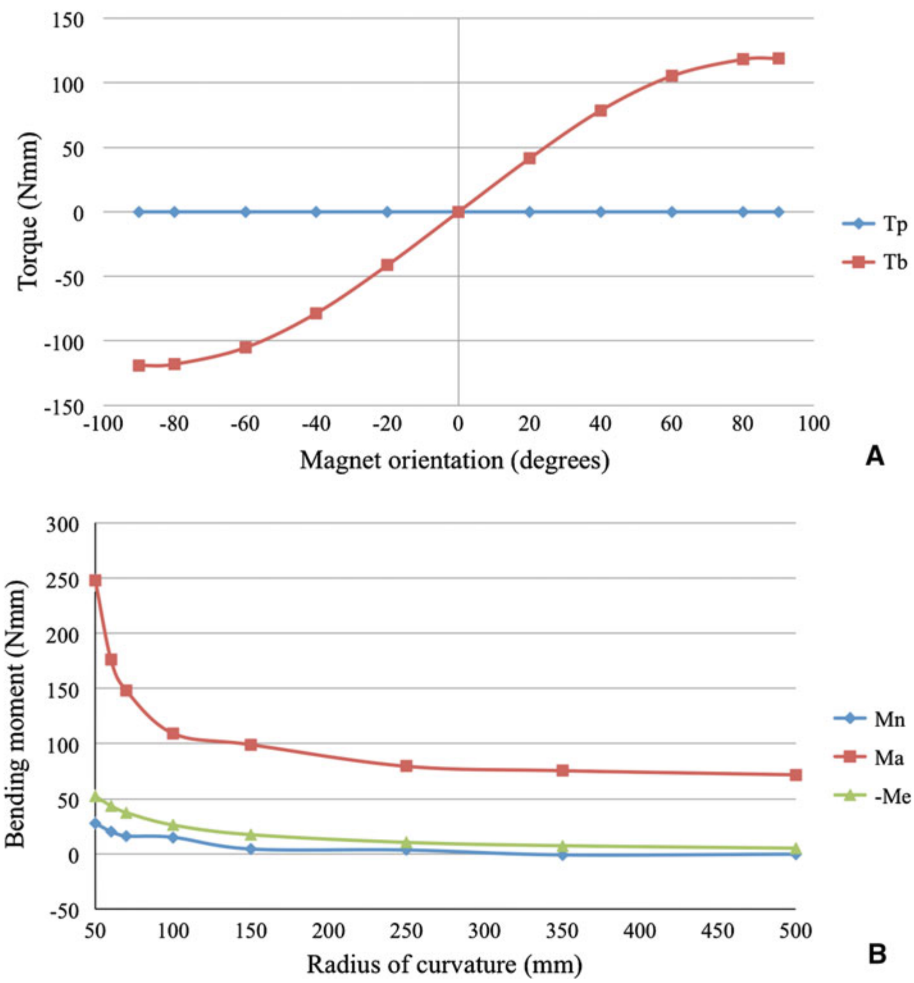

generating a magnetic moment that produces the bending of the passive vertebrae (Fig. 4d). The servomotor controls the magnitude of the bending moment and its direction (left or right) by modifying the orientation of the magnets (β angle) in the active vertebra. As previously mentioned, as opposed to a robot where the movements are mainly enforced by servomotors, the proposed magnetic actuator has the advantage of generating a force as direct output. This design allows the robot to have a natural behaviour responding to both the internal actuation and the external interaction with the water.

The performance of the actuator was evaluated through finite element analysis. This analysis calculated the torque required by the servomotors to modify the orientation of the active magnets. Additionally, it assessed the bending moment provided by the active segment. Figure 5a shows the torque required by the servomotors to modify the orientation of the two active magnets when the vertebrae are parallel (T_p) or in the maximum bend configuration (T_b). When the vertebrae are parallel (straight segment), the rotation of the active magnets is self-balanced ($T_p = 0$) due to the specific magnetic layout. Indeed, when the three vertebrae are parallel, the torque on the magnet a.1 compensates the torque on the magnet a.2 during the rotation of the shaft. This design ensures that the energy provided by the DC motor to modify the orientation of the magnets is almost completely used to bend the vertebrae in order to achieve locomotion (part of the energy is lost due to friction between mechanical elements). In other terms, the specific magnetic layout uses energy only for net output mechanical work, and near-zero energy is lost for magnets orientation. The torque evaluated when the vertebrae are fully bent (T_b) represents the maximum torque required by the servomotor. Figure 5b reports the value of the magnetic moment in the active segment as a function of its radius of curvature, when the magnets are either in neutral (M_n) or in maximum attraction (M_a) configuration. In Fig. 5b, also the value of the elastic bending moment ($-M_e$) generated by the flexible notochord is presented. The graph shows that the neutral position is unstable since M_n facilitates the bending of the vertebrae. However, the stability of the neutral configuration is achieved by ensuring the condition below:

$$M_n < -M_e < M_a \quad (1)$$

The notochord stabilises the vertebrae, ensuring their parallelism and alignment when the magnets are in the neutral configuration. Meanwhile, the attraction configuration of the magnets causes the complete bending of the segments.

Swimming locomotion is characterised by a periodic movement of the segments of the robot with cyclical accelerations and decelerations. The synergy between the elastic notochord and the compliant magnetic actuators increases the actuation efficiency of the robot by exploiting the passive dynamics of the robot. During the deceleration phase, the kinetic energy of the segments is stored in the elastic notochord and into magnetic regions where repulsive forces occur, and it is then released during the acceleration phase. Both the elastic behaviour of the body and the conservative nature of the magnetic forces imply that the robot has a natural swimming frequency, which maximises the swimming efficiency of the system. The natural frequency of the artefact results from physical characteristics of the artefact's body, from the intrinsic compliance of the magnetic actuator and the interaction of the body with water during swimming. The main characteristics of the body that influence natural frequency are the mass of the vertebrae and the stiffness of the notochord. The natural frequency increases if the stiffness of the notochord is higher and decreases if the robot is heavier. Permanent magnets behave similarly to nonlinear springs, and they also contribute to the natural frequency of the whole robot. Finally, since the robot displaces water during swimming, added mass reduces the natural frequency. The natural mechanical frequency of the artefact has been experimentally evaluated to be around 0.6 Hz as illustrated in Fig. 10.

As shown in Fig. 6, the robot is equipped with two stretch receptors (left and right) for each adjacent vertebra in order to measure the local curvature of the body. The stretch receptors are optical sensors composed of an infrared-emitting (a) and a receiving diode (b) connected to dedicated electronic boards, (g) in Fig. 4. The diodes are enclosed inside a soft black silicone tube as shown in Fig. 6, which prevents the external light interfering with the measurements. When the vertebrae bend, the silicon tube is stretched, reducing transmitted light and causing a variation in the signal acquired by the receiver.

A waterproof and compliant "skin" covers the artefact. It provides some elasticity, thus providing bending stiffness in addition to the elastic notochord. However, this membrane only slightly affects the dynamics of the robot since it is composed of very soft and thin layers of silicone. Each layer is separated by means of a film of hydrophobic lubricant in order to improve waterproofing and crack resistance. Indeed, the hydrophobic layers act as a release agent, thus reducing the risk of crack propagations.

The tail is made of a fibreglass-reinforced polymer, showing little hysteresis and experimentally tailored passive compliance. As demonstrated by Park et al. (2012), a tail with a tailored compliance maximises swimming thrust and, therefore, the robot's performance.

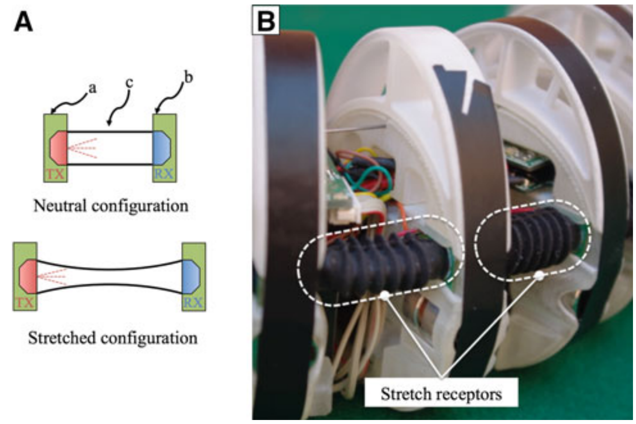

Fig. 6 Overview of the stretch receptors. **b** shows a picture of three consecutive vertebrae with their stretch receptors. **a** shows the working principle of each stretch receptor: it is composed of two electronic boards, one with an emitter diode (*a*) and one with a receiver (*b*). The electronic boards are connected to the vertebrae of the robot as shown in Fig. 4a, b. The sensors are embedded inside a silicone tube (*c*) in order to reject possible interference from external light sources. In **b** a close view of the vertebrae shows the integration of the stretch receptors. The stretch receptor on the right is in the neutral configuration, while the one on the left is stretched

3.2 Control system and local network communication

Biological systems rely on distributed neural networks systems, which are involved in locomotor behaviour such as swimming and walking. This distributed organisation allows the biological system to achieve fast responses using peripheral reflexes reducing the "computational burden" of the brain. This biological structure inspired the control system design for the presented artefact. The control of the robot is composed of seven low power consumption electronic boards as shown in Fig. 7: one in the head, named *head-board* (HB), five along the body, named *segment-board* (SB), and one on the tail, named *wireless board* (WB). An external console (EC) implements more complex behaviours (high-level control) involved in the visual process, and it monitors and controls the parameters of the robot such as voltage, sensor information and motor control. The external console is involved in the implementation of more complex biological behaviour, which cannot be implemented in the robot due to low on-board computational burden. Figure 8 highlights how the vision control loop is implemented by exploiting the *external console* in order to process the images streamed by the artefact.

The design of each electronic board is the result of a tradeoff between mechanical design, available space and computational performance required to implement the control system. Each electronic board includes a Microchip DSP 16 bit

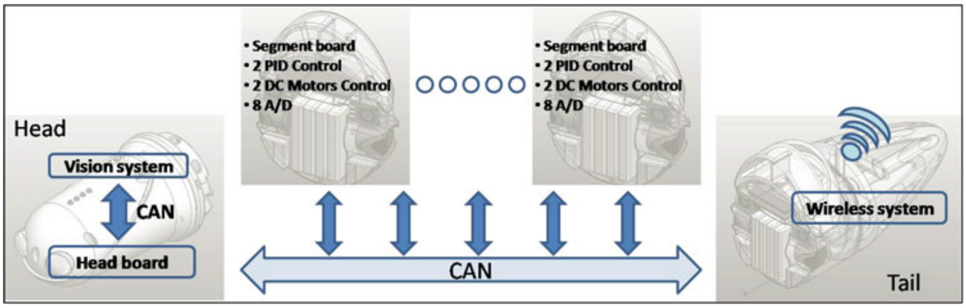

Fig. 7 Control hardware architecture embedded in the lamprey-like robot. The control hardware is composed of seven electronic boards distributed along the body: five *segment-boards*, one *head-board* and one *wireless board* involved in the wireless communication. Each *segment-board* controls two segments and creates a local proportional, integrative and derivative (PID) control to impose the position or the velocity for each segment. Each *segment-board* has 8 A/D (analogue to digital) converters to acquire the sensors of the angle of the segment. All the boards communicate by means of a CAN bus

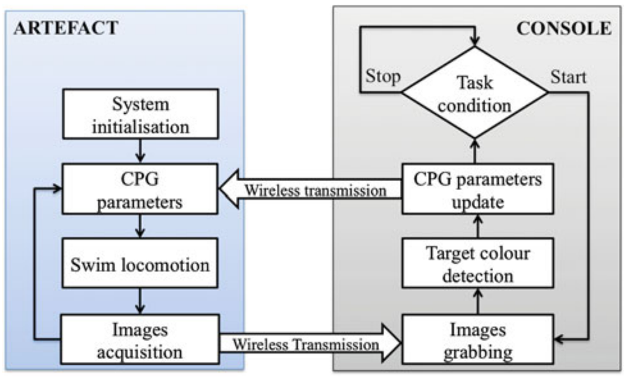

Fig. 8 Vision control loop. The figure illustrates the control algorithm loop. The artefact platform performs the swimming behaviour autonomously by streaming a stereoscopic video to the external console. The external console calculates the position of the target in the field of view of the robot and sends the new CPG parameters to the robotic platform. Start and stop conditions change according to the tasks. Examples of start–stop conditions are swim/rest command or target visible/target reached

and a power supply chip, which stabilises the voltage level provided from the battery supply to 3.3V. The voltage signals from the Control Area Network (CAN) bus used to communicate between the segments are converted by means of a dedicated chip (Microchip MCP2200), which is involved in both signal noise rejection and differential signal transmission. The *segment-boards* include, in addition, two standard H-bridge motor drivers in order to control two DC motors. The *wireless board* uses a Microchip MRF24J40, which implements a wireless serial communication at 2.4 GHz with a bandwidth of 1 Mbit/s.

The *head-board* represents the middle-level control of the system. It is involved in the monitoring of the segments and, together with the *wireless board*, represents a bridge between the *external console* and the robotic platform. The *head-board* sets all the new control parameters to the *segment-board* where the low-level control is implemented.

Both the middle- and low-level controls are involved in the management of the artefact in order to perform autonomous tasks. The platform can be controlled in two methods: (i) remotely, by means of an external graphical interface and a joy-pad; and (ii) autonomously, by implementing a goal-directed locomotion behaviour, by using the vision sensor and by targeting an external target. In the first method, the users can control the artefact by setting different commands such as start, reverse swimming, turn and stop. This is important to control the robotic platform during both demonstrations and experiments. The second method allows the robot to be autonomous, and due to the high computational burden, it is used to implement more complex behaviours involving the vision system.

The boards inside the artefact are connected together by means of a local network communication, which relies on a CAN serial bus. This bus is widely used in automotive and industrial control because of its reliability, high immunity from external noise and the simplicity of its cabling.

The signal transmission uses a differential codification, and it is composed of only two wires, named CANH and CANL. The communication protocol can be either configuration, such as multi-master or multi-slave. This bus is suitable for replicating a neural network communication system because it can simulate the neural interconnections.

The cabling for the communication and the power supply is located in the dorsal side of the artefact like an artificial spinal cord. This solution simplifies the cabling of the artefact, and it prevents the wires from being stretched because of body movement of the artefact. This bioinspired artificial spinal cord handles afferent and efferent signals implementing a distributed and decentralised control. The afferent signals are represented in the artefact by the sensors detecting the angle/curvature between each segment as described in Fig. 6.

This distributed control allows the robot to be a useful tool to study biological models because it is able to replicate different models of CPG due to each *segment-board* having a dedicated Digital Signal Processor (DSP), which can replicate local neural networks. The local communication network of the robot represents the neural connection, and the *head-board* represents the locomotor control, which is involved in the swimming pattern selection.

Several models of CPG have been proposed within a swimming platform (Ijspeert 2008). Our model consists of a network of phase oscillators, reported in Ijspeert (2008), which can be represented in the following differential equations:

$$\dot{\varphi}_i(t) = 2\pi \nu_i + \sum_{j=0}^{N-1} \omega_{ij} \sin\left(\varphi_j\,(t) - \varphi_i\,(t) - \phi_{ij}\right)$$
$$\varphi_i(0) = \varphi_{i0}, \quad i = 0, ..., N-1, \ t \geq 0 \tag{2}$$
$$\ddot{r}_i(t) = -2\varsigma\omega_n \dot{r}_i(t) + \omega_n^2(\alpha_i - r_i(t))$$
$$r_i\,(0) = r_{i0}, \quad \dot{r}_i(0) = \dot{r}_{i0} \tag{3}$$
$$\theta_i(t) = r_i(t)cos(\varphi_i(t)) + \Delta_i(t) \tag{4}$$

where $\varphi_i(t), r_i(t), \theta_i(t)$ represents the phase, the oscillation amplitude and the angle of the joint i, ω_{ij} represents the weight of the phase of joint j on that of joint i, ϕ_{ij} is the desired steady-state phase difference between segments i and $j, \varsigma, \omega_n > 0, \alpha_i$, is the desired steady-state amplitude of oscillation of segment i, ν_i represents the desired steady-state oscillation frequency, and N is the number of the segments. In the presented work, we assumed the following rules:

$$\omega_{ij} = 0 \quad \text{if } j = 0, ..., N-1 \quad \text{otherwise} \quad \omega_{ij} = \omega,\ j = i \pm 1 \tag{5}$$

$$\nu_i = \upsilon \tag{6}$$
$$\phi_{ij} = \frac{2\pi S}{N}, \quad \text{if } j = i - 1$$
$$\phi_{ij} = -\frac{2\pi S}{N} \quad \text{if } j = i + 1 \tag{7}$$
$$\phi_{ij} = 0 \quad \text{otherwise}$$

where S is the number of sinusoids described by the shape of the robot.

In Eq. (4), the variable $\Delta(t)$ allows the robot to steer left and right by adding an offset at the oscillation amplitude of the vertebrae. This offset imposes a local curvature in the body, which is propagated from head to tail. As described later, this control variable changes according to the target inputs from the visual system.

The *head-board* sets the oscillation wave for each *segment-board,* and each *segment-board* is able to keep its oscillation by itself controlling the oscillation (amplitude, frequency and offset from zero position) of the permanent magnets (β angle) and closing a local loop within the local sensors such as the sensors of the angle of each segment.

In order to improve both the quality of the video streaming and the capability to maintain a target in the field of view of the cameras, the oscillation of the head is reduced by imposing an opposite phase only at the first, as reported in the equation below:

$$\theta_i(t) = -r_i(t)\cos(\varphi_i(t)), \quad i = 0 \tag{8}$$

3.3 Vision system

A common characteristic of living organisms is the capability to sense the surrounding environment acting and moving dexterously in known or unknown spaces. The presented vision system is relevant in the evaluation of the neuroscientific models and goal-directed behaviour in the lamprey animal.

The sense of sight in the lamprey is strictly related to the locomotion patterns (Saitoh et al. 2007), and it is directly involved in the selection of behaviour during swimming. The vision system is composed of two 2D CMOS cameras, MO-S3588-2G-N from Misumi. These cameras are mounted with an overlap angle of 30° in relation to the sagittal plane. Together, the overlap angle and the fish eye lenses mounted on the cameras allow the robot to achieve a field of view of up to 150°.

Figure 9 describes the vision system. Two cameras stream the video at 30 frames per second to the *external console*.

The software implemented in the external console is written in C#. The image-processing algorithm detects both the position and the mass of the target object in the camera reference system. The position of the target is in pixels, and the mass is represented as the number of pixels detected. These data are used to control the turning rate of the artefact by modulating the main CPG parameter such as the offset of the amplitude. The target is detected using a standard OpenCV library (Bradski and Kaehler 2008) for image detection.

The new offset ($\Delta(t)$ in Eq. 4) for the oscillation angle of the vertebrae is calculated as below:

$$\Delta = k \cdot (\alpha D_\mathrm{l} \cdot P_\mathrm{l} - \alpha D_\mathrm{r} \cdot P_\mathrm{r}) \tag{9}$$

where k and α are normalised coefficients, and D_l, $D_{\mathrm{r},}$, P_l and P_r are the dimensions and the centre of mass in pixels of the target, on the image left and right, respectively.

This control rule allows the robot to follow and reach a target. If k becomes negative, the robot avoids the target by turning in the opposite direction.

3.4 Energy consumption

Energy consumption is one of the major issues in the design of autonomous robots. This limitation determines the operation time. In an autonomous platform, the energy consumption is distributed between actuators, embedded digital control, the vision system and the computational burden

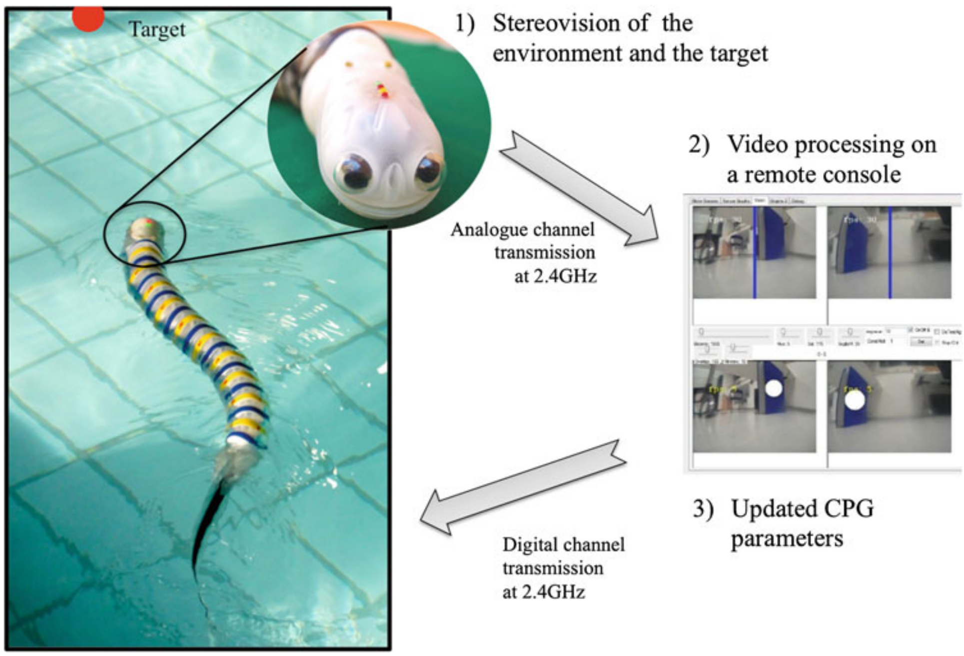

Fig. 9 Vision control loop implementation. The figure illustrates the implementation of the control loop and its block scheme as reported in Fig. 8. The videos of the cameras are streamed to the external console involved in the video processing (an example of the graphical unit interface is shown in step 2 of the picture). The wireless communication system of the robot is composed of two transmitters. The first one is involved in the video streaming and is located in the head (*1*). The communication transmission protocol is analogue at the frequency of 2.4 GHz. The second uses a digital communication protocol at the frequency of 2.4 GHz and streams the data to control the platform such as the sensors, the motor control and the parameters of the CPG. This is located in the tail in order to avoid noise in the communication (*3*)

Table 1 Features of the robot in terms of power consumption and mechanical performances

Robot size	Length 990 mm, diameter 54.5 mm
Swimming speed	Up to 0.25 body length per second
Power consumption (Pwc)	Up to 8 W
Control board (Pwc)	2 W
Wireless board	0.2 W
Vision system (Pwc)	0.28 W $\times 2 = 0.56$ W
Actuators (Pwc)	Up to 0.4 W $\times 10 = 4$ W
Bending radius	75 mm
Weight	1,640 g
Number of DSP	7
Run time	Up to 5 h

needed to replicate the biological model. In order to reduce the energy involved in the computational burden, as described above, the vision system algorithm is processed in an external console.

The energy source of the robot relies on ten battery packages connected in parallel and located along the entire body in order to achieve a uniform distribution of the weight. Each package is composed of four parallel 3.7 V lithium batteries with an energy capacity of 1,120 mAh. The total capacity is about 10.5 Ah. This design allows the robot to swim up to 5 h with an average speed of 0.25 body length per second using an average power of 10 W. Table 1 reports the energy consumption of the robot referring to each subsystem of the robot and mechanical performances.

4 Experiments, testing and performances of the artefact

The high energy efficiency of the system allows the team to perform lengthy experiments extending up to 5 h.

A number of experiments were carried out in water within different experimental set-up contexts. The robotic platform was also able to perform object tracking tasks consisting of avoiding or following light or objects. Indeed, the artefact is able to respond to an external visual stimulus by changing its behaviour such as combining the swimming locomotion pattern with turning movements.

Preliminary experiments were performed in order to optimise the swimming of the robot and to identify the natural frequency of the flexible body, which maximised the locomotion performance, in terms of speed, while reducing the energy consumption. As for the identification of the best swimming parameters, the wavelength of the propagated wave along the body of the robot, the amplitude and frequency of oscillation of the magnets while performing forward swimming and turning have been determined. Finally, a procedure for head stabilisation control (HSC) was tested in order to facilitate the ability to follow and reach an object.

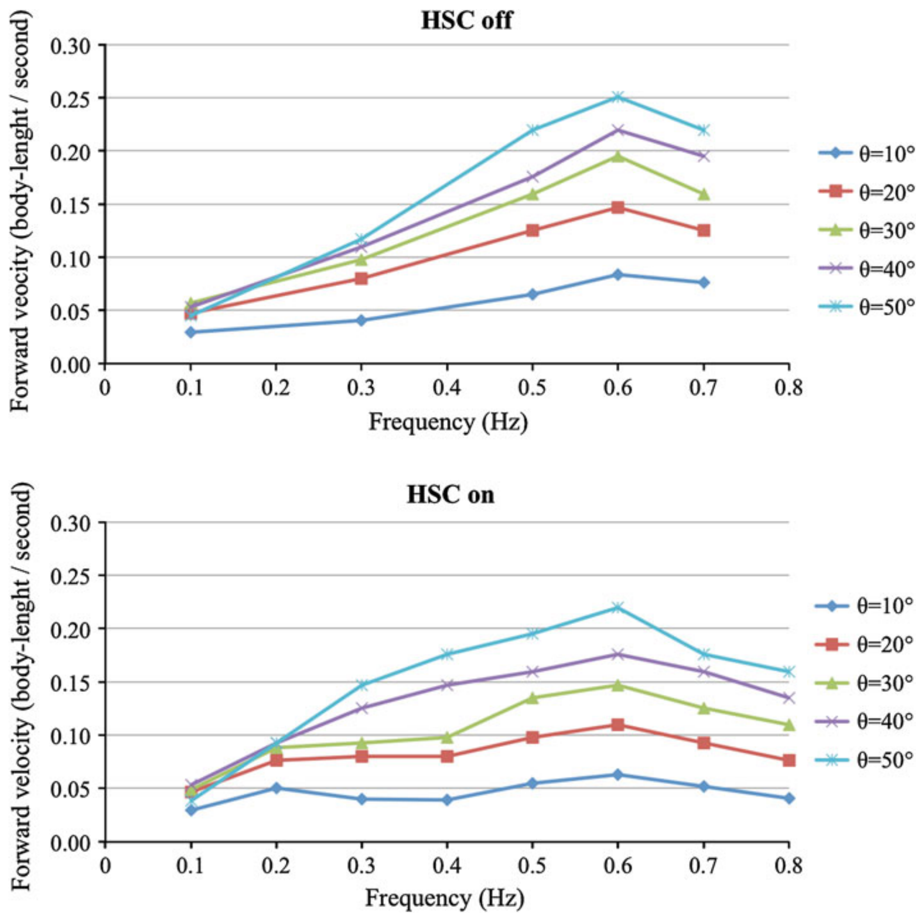

Fig. 10 Forward velocity (body length/second) of the artefact achieved using different oscillation frequencies (Hz) and amplitudes of the magnets (angle β in Fig. 4). All trials started with the artefact located in one side of the pool. The *top graph* describes the experiments with the HSC off, while in the *bottom graphs*, it was on. Both graphs report the forward velocity locomotion in an undirected behaviour

Trials were carried out in air with the artefact suspended in order to study the behaviour of the flexible body of the robot. Each vertebra was attached to a horizontal frame with a thin, long string to constrain the vertical movement of the artefact while maintaining enough freedom for oscillation of the body. The tests in the air aimed to investigate the response of the platform to different locomotion parameters, to calibrate the stretch sensors and to debug the control algorithms. The robot swims due to a synchronised oscillation of the magnets in each active vertebra, which generates a rostro-caudal travelling wave. The intersegmental delay of segment activation, the amplitude and frequency of magnet oscillation are the main locomotion parameters that control the motion. Tests in air highlighted the behaviour of the mechatronic platform in relation to the changes of the control parameters such as $\varphi_i(t)$, $r_i(t)$, $\theta_i(t)$ and S.

After debugging both the control system and the mechanics, the robotic platform was tested in water in order to characterise the natural frequency of the artefact during forward swimming. Trials with different frequencies and oscillation amplitude of the active segment (angle β in Fig. 5) were performed in order to measure the forward velocity of the robot. Figure 10 summarises the results of the test and reports the resonant frequency of the robot in an undirected behaviour, which is 0.6 Hz. Furthermore, the forward swimming velocity of the artefact increases with the amplitude oscillation of the magnets.

Extensive tests were carried out to evaluate the performance of the robot when it swims with the HSC on (Eq. 8).

The experiments proved that the oscillation of the head needed to be reduced in order to facilitate object tracking during swimming. This phenomenon was related to the difficulty for the visual system in detecting and maintaining the target in the field of view of the cameras. Additionally, the swimming movement is wave generated and propagated from the head to tail. Comparing these results to the previous experiments on forward swimming, the graphs in Fig. 10 show a similar response to the locomotion parameters. However, when the HSC was on (bottom graph), swimming velocity was lower than when the HSC was off (Fig. 10 top graph). In the real animal, the orienting movements of eyes, neck and trunk are elicited by the same command centre, the optic tectum (i.e. the homologue of superior colliculus in mammals). Intensity and location of the activation of the optic tectum determines the pattern of response. Therefore, lamprey is able to swim in the direction of the gaze with a very short delay between the activation of orienting movements and the initiation of locomotion (Saitoh et al. 2007). Efficiency of this self-regulated

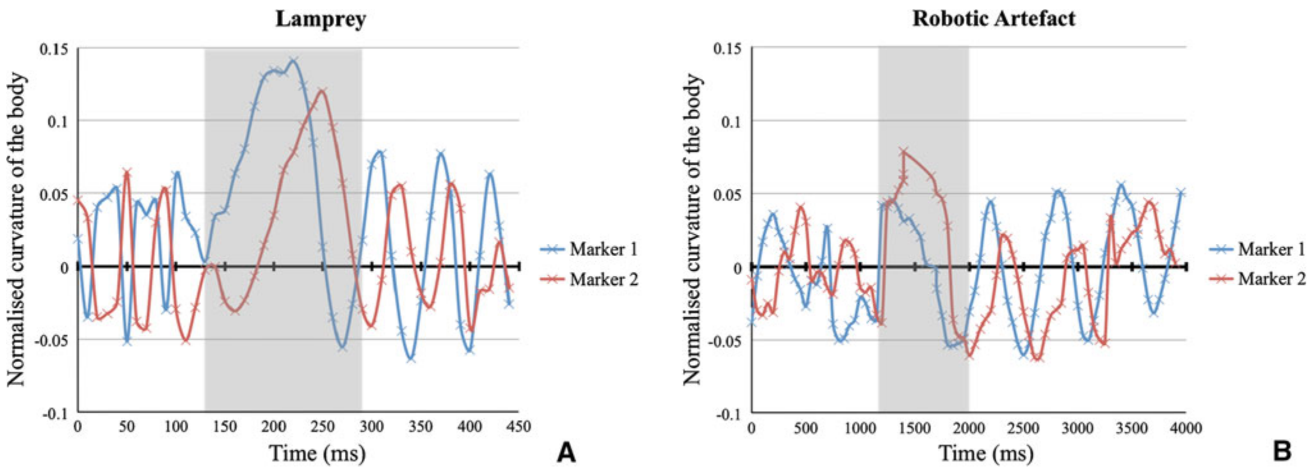

Fig. 11 Comparison between the steering capabilities of the lamprey and of the artefact during a left turning episode. These images report the tracking of two markers one rostrally and one caudally positioned, respectively, marker 1 and marker 2. The animal was about three times faster than the robot

system of targeting is also made possible due to the anatomical configuration of the head and neck of the lamprey. In fact, even if head, neck and trunk show a certain degree of independence, a movement of one part will result in a movement of the other sections.

Final tests were focused on the steering capabilities of the artefact. The robot can steer and efficiently turns like its biological counterpart. Steering capabilities allow the robot to make U-turns in less than a metre square. Figure 11 shows a qualitative comparison of the body curvature of both the lamprey and the artefact during a left turning episode.

Motion analysis of the turning behaviour was made using a high-speed digital camera (CASIO EXILIM High Speed EX-FH25) and analysed by image tracking software (ProAnalyst® Professional Edition). All videos were recorded from above during free-swimming behaviour in the swimming pool. To track the movements, both lamprey and artefact were equipped with a set of markers along the dorsal side of the body as reported in (Islam et al. 2006).

The reported dynamic data were used to calibrate the parameters of the CPG control, that is, the amplitude, phase shift and frequency of the sinusoidal locomotion movements.

The movement frequency of the swimming lamprey ranges from 0.5 to 10 Hz, but the current version of the lamprey robot is not able to reach the full range of frequencies of its biological counterpart. Table 2 reports a comparison between lamprey (with reference to a particular species *Lampetra fluviatilis*) and the robot (Hardisty 1986; Hardisty and Potter 1971; Laine et al. 1998). Despite this limitation, after the first experimental session in air, the swimming parameters were modified in order to maximise the performance of the robot: the maximum swimming speed was 0.25 body lengths per second (bls) obtained with a frequency of 0.6 Hz and a wavelength of 1.2 m.

Table 2 The lamprey and the robot

	Lamprey (*Lampetra fluviatilis*)	Artefact
Body length (mm)	200–400	990
Diameter (mm)	20–80	54.5
Body weight (g)	60	1,640
Swimming velocity	110 (cm/s)	0.25 (bls)

Comparison between the real animal and the robotic artefact

Additional experiments were performed in order to investigate the goal-directed locomotion driven by visual stimuli. The visual input from the two cameras on the head produces a stereo image, which was processed and used to control the swimming direction of the artefact. Goal-directed locomotion can be achieved by using very simple rules (such as distinction between targets or obstacles) by detecting the target position via the visual input.

Experiments with the artefact and lamprey were performed in two different swimming pools. The pool for the animal was one metre in diameter. The pool for the robot was three and half metres in diameter. Each swimming pool was equipped with two lights placed into the water in diametrically opposite directions. When one light was switched on, the artefact was able to recognise the visual stimulus and follow it. When the robot reached the light on one side of the pool, the visual stimulus was switched off and the light positioned in the opposite side was switched on. The robot was able to find the opposite light by turning on itself until a new visual stimulus was detected. This resulted in the robot turning and crossing the pool from one side to the other. All the trials were recorded with a webcam (Microsoft®, wide angle F/2.0, 720 pHD, 30 fps). Videos collected were used to measure the swimming parameters. Figure 12 shows two snapshots of the set-up.

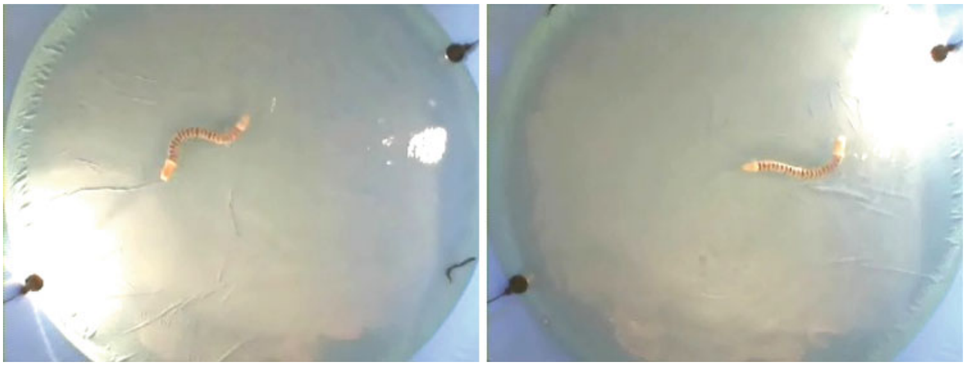

Fig. 12 Experimental set-up of object tracking. Snapshots extracted from video recordings made during the experimental session of object tracking show the artefact in two different moments during the fulfilment of the task. The light recalls and activates the goal-directed behaviour. The robot swims towards the left light (*left snapshot*), and then the light is switched off. The right light is switched on, and after a few moments of free swimming and searching patterns (simple turns), the new target falls within the field of view (*right snapshot*)

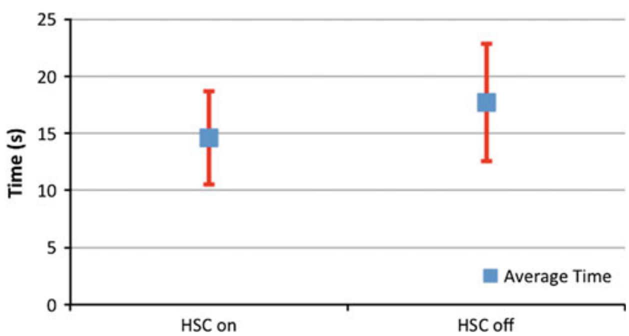

Fig. 13 Time performance in object tracking. Object tracking was performed and compared when the head stabilisation control (HSC) was in both configurations, on and off. When the HSC was on, the average time was less than when it was off, 14.6 and 17.7, respectively. The standard deviation with the HSC on was less than when the HSC was off. This reports a robustness of control with the HSC on, enabling it to keep tracking the target

The light-pursuing tasks were performed with the HSC on and off, in order to explore the relevance and effectiveness of this control during goal-directed behaviour.

Several trials were performed in order to compare the performance of the visual control to reach the target. We performed fifteen trials with the head stabilisation control (HSC) on and another fifteen with the HSC off, the start configuration was with the robot in front of the object, with the target detected by the vision control. The experiment reported an average time and a standard deviation of 14.6 and 4.11 s when the HSC was on and 17.7 and 5.15 s when it was off (Fig. 13). These results highlight the relevance of the HSC to track and reach a target. While the HSC was on, it permitted the image processing to achieve a stable detection of the target allowing the platform to reduce the time to reach the target and never lose the target from the field of view. In contrast, with HSC off, the artefact lost the target from its field of view in four of the fifteen trials, resulting in intentional extra turns in order to find the target again. This behaviour explains both the higher mean value and standard deviation.

Table 3 Robustness of the HSC control

	Performance with the target lost	Performance without the target lost
HSC on	0	15
HSC off	4	11

We have reported the number of times where the artefact lost the target with the HSC on and off. These data report an improvement of the robustness of the control when the HSC is on, allowing the robot to keep the target in the field of view avoiding the need to twist on itself to find the target again

We have analysed the results of the experiments using Fisher's exact test. We have evaluated the robustness of the system with the data reported in Table 3.

The statistical test reports a value of $p = 0.096$ which is almost statistically significant. We can conclude that the HSC control improves the robustness of the artefact keeping the target in the field of view.

5 Discussion and perspectives on the potential of the synergy between robotics and neuroscience

This paper introduced and described a novel robotic platform as a tool for biological model validation. The mechanical system is designed to be compliant in order to achieve a natural interaction with the external environment during locomotion. The distributed control is designed in order to implement a control system for the biological models. The vision system is able to process the video streaming and to implement a more complex biological system, including goal-directed locomotion driven by visual input. The external console is involved in the image processing and reduces the computational burden of the control system embedded in the platform. The artefact is controlled according to locomotion parameters (i.e. swimming body frequency and speed) based on the behaviour of the real animal. The similarity between the lamprey and the artefact enables the validation of the neural models for goal-directed locomotion. In the light-tracking task, the behaviour of the artefact, as in the lamprey, is driven by external visual stimuli, which affect the CPG parameters active in the moment. We have presented a control system able to stabilise head movements during swimming. We are planning to integrate more sensors, such as inertial systems, in order to implement more complex behaviours. In lampreys the postural control during locomotion is mediated either by visual or by vestibular inputs that contribute to stabilise the position of the body and of the head on all three planes (horizontal, sagittal and transverse). Visual stimuli elicit the response of eye, neck and trunk and can have a modulatory effect on locomotion: the animal is thus able to target objects thanks to body and head-related movements. The driving of postural control occurs also thanks to the fundamental contribution of the vestibular system. In fact, damages or lesions to the vestibular system cause motor disorders, including abnormal eye positions and asymmetry of the head and trunk position.

The robotic platform enables a biohybrid approach to animal experiments: interfacing the artefact with the real animal in order to directly tune internal parameters of the hardware based on ongoing neural activity in the animal, making it possible to explore in more detail goal-directed locomotion. The proposed idea consists of in vivo experiments in which the isolated brainstem of the lamprey is bidirectionally connected to the artefact. Activities of the main descending motor pathways will be recorded and sent in real time to the CPG models of the robotic artefact. The principal motivation for this activity is that intracellular recordings in freely moving animals are of key importance but are also difficult to perform; by using a freely moving artefact with a CPG on board, it may be possible to decouple the natural central nervous system and perform locomotion while performing neurophysiological measurements and manipulations.

The biohybrid approach could improve the quality of investigation on the motor pathways as the expression of a particular locomotor program and the CPG models in a feedback loop using their implementation in the artefact.

Indeed, advantages introduced by this kind of experiment include several possibilities. It could be possible to measure the activity of the descending motor commands, with the direct verification of control hypotheses during steady-state locomotion, compared to non-steady-state locomotion. Additionally, we can explore interaction of the different sensor modalities when they are in action, and by disturbing some modalities and not others, we can see how it affects locomotion behaviour. To achieve these results, it will be necessary to further develop the recording methodology from the animal, in particular concerning filtering, resolution and reproducibility.

Acknowledgments The work presented in this manuscript was supported by the European Commission (FP7) within the framework of the LAMPETRA Project (EU contract no 216100). The authors would like to thank Mr Riccardo di Leonardo, Engineer Roberto Lazzarini, Mr Gabriele Favati, Mr Andrea Melani and Engineer Nicodemo Funaro for their advice and help in the fabrication of part of the robot. Finally, thanks to Mr Godfried Jansen van Vuuren for his technical support and many thanks to Lorna Gracie.

Conflict of interest The authors declare that there is no conflict of interest or competing financial interest related to the work described.

References

Albu-Schaffer A, Ott C, Hirzinger G (2007) A unified passivity based control framework for position, torque and impedance control of flexible joint robots. Int J Rob Res 26(1):23–39

Arkin RC (1998) Social behaviour. In: Behaviour-based robotics. MIT Press, Cambridge, Massachusetts

Ascari L, Bertocchi U, Corradi P, Laschi C (2009) Bio-inspired grasp control in a robotic hand with massive sensorial input. Biol Cybern 100(2):109–128

Ayers J, Wilbur C, Olcott C (2000) Lamprey robots. In: Wu, T, Kato, N (ed) In: Proceedings of the international symposium on aqua biomechanisms. Tokai University

Bar-Cohen Y (2012) Nature as a model for mimicking and inspiration of new technologies. Int J Aeronaut Space Sci 13(1):1–13

Barranco F, Diaz J, Ros E, Del Pino B (2009) Visual system based on artificial retina for motion detection. Trans Cybern IEEE 39(3):752–762

Beer RD, Quinn RD, Chiel HJ, Ritzmann RE (1997) Biologically inspired approaches to robotics. Commun ACM 40(3):31–38

Bradski G, Kaehler A (2008) Learning openCV computer vision with the openCV library. O'Reilly Media, USA

Chiel H, Ting L, Ekeberg Ö, Hartmann M (2009) The brain in its body—motor control and sensing in a biomechanical context. J Neurosci 29:12807–12814

Crespi A, Ijspeert AJ (2009) Salamandra robotica: a biologically inspired amphibious robot that swims and walks.In: Springer (ED) Artificial life models in hardware, pp 35–64

Durr V, Schmitz J, Cruse H (2004) Behaviour-based modelling of hexapod locomotion: linking biology and technical application. Arthropod Struct Dev 33(3):237–250

Ekeberg Ö (1993) A combined neuronal and mechanical model of fish swimming. Biol Cybern 69:363–374

Ekeberg Ö, Grillner S (1999) Simulations of neuromuscular control in lamprey swimming. Philos Trans R Soc Lond B 354:895–902

Grillner S (2003) The motor infrastructure: from ion channels to neuronal networks. Nat Rev Neurosci 4:573–586

Grillner S, Graybiel AM (2006) Microcircuits—the interface between neurons and global brain function. Massachusetts MIT Press, Cambridge

Grillner S, Jessell TM (2009) Measured motion: searching for simplicity in spinal locomotor networks. Curr Opin Neurobiol 19:572–586

Grillner S, Kozlov A, Dario P, Stefanini C, Menciassi A, Lansner A, Kotaleski JH (2007) Modeling a vertebrate motor system: pattern generation, steering and control of body orientation. In: Cisek P, Drew T, Kalaska JF (eds) Progress in brain research, vol 165. Elsevier, pp 221–234. ISSN 0079-6123, ISBN 9780444528230

Hardisty MW (1986) Petromyzontiforma. In: Holcik J (ed) The freshwater fishes of Europe. Aula-Verlag, Wiesbaden

Hardisty MW, Potter IC (1971) The biology of lampreys. Academic Press, London

Hirose S, Yamada H (2009) Snake-like robots [Tutorial]. Rob Autom Mag IEEE 16(1):88–98

Hochhalter D (2011) Artificially produced spider silk fibers as a high tech biological material. Basic Biotechnol 7:12–16

Hu Y, Katragadda RB, Hongen T, Zheng Q, Li Y, Xu Y (2010) Bioinspired 3-D tactile sensor for minimally invasive surgery. J Microelectromech Syst 19(6):1400–1408

Hunter I, Lafontaine S (1992) A comparison of muscle with artificial actuators. In: Workshop solid state sensors actuators, 5th technical digest IEEE 22–25 June 1992, pp 178–185

Ijspeert AJ (2008) Central pattern generators for locomotion control in animals and robots: a review. Neural Netw 21(4):642–653

Islam SS, Zelenin PV, Orlovsky GN, Grillner S, Deliagina TG (2006) Pattern of motor coordination underlying backward swimming in the lamprey. J Neurophysiol 96:451–460

Kawato M (2000) Robotics as a tool for neuroscience: cerebellar internal models for robotics and cognition. In: Hollerbach MH, Koditschek DE (eds) Robotics research. The ninth international symposium. Springer, London, pp 321–328

Laine A, Kamula R, Hooli J (1998) Fish and lamprey passage in a combined Denil and vertical slot fishway. Fish Manag Ecol 5(4):31–44

Li F, Liu W, Fu X, Bonsignori G, Scarfogliero U, Stefanini C, Dario P, (2012) Jumping like an insect: design and dynamic optimization of a jumping mini robot based on bio-mimetic inspiration. Mechatronics 22(2):167–176. ISSN 0957-4158

Madden JDW, Vandesteeg NA, Anquetil PA, Madden PGA, Takshi A, Pytel RZ, Lafontaine SR, Wieringa PA, Hunter IW (2004) Artificial muscle technology: physical principles and naval prospects. Ocean Eng IEEE J 29(3):706–728

Manfredi L, Maini ES, Dario P, Laschi C, Girard B, Tabareau N, Berthoz A (2006) Implementation of a neurophysiological model of saccadic eye movements on an anthropomorphic robotic head. Humanoid Robots, 6th IEEE-RAS international conference on, pp 438–443

Manfredi L, Maini E S, Laschi C (2009) Neurophysiological models humanoid robotics of gaze control in humanoid robotics. In: Choi B (ed) Humanoid robots, pp 187–212

Mazzolai B, Mondini A, Corradi P, Laschi C, Mattoli V, Sinibaldi E, Dario P (2011) A miniaturized mechatronic system inspired by plant roots for soil exploration. Trans Mechatron IEEE/ASME 16(2):201–212

Ott C, Albu-Schaffer A, Kugi A, Hirzinger G (2008) On the passivity based impedance control of flexible joint robots. IEEE Trans Rob Autom 24(2):416–429

Park Y, Jeong U, Lee J, Kwon S, Kim H, Cho K (2012) Kinematic condition for maximizing the thrust of a robotic fish using a compliant caudal fin. Rob IEEE Trans 28(6):1216–1227

Pfeifer R, Iida F, Bongard J (2005) New robotics design principles for intelligent systems artificial life, vol 11. MIT Press, Cambridge MA USA

Pratt G, Williamson M (1995) Series elastic actuators. In: Proceedings IEEE/RSJ international conference on human robot interaction and cooperative robots, vol 1, pp 399–406

Rovainen CM (1979) Neurobiology of lampreys. Physiol Rev 59:1007–1077

Saitoh K, Menard A, Grillner S (2007) Tectal control of locomotion, steering, and eye movements in lamprey. J Neurophysiol 97(4):3093–3108

Scarfogliero U, Stefanini C, Dario P (2009) The use of compliant joints and elastic energy storage in bio-inspired legged robots. Mechan Mach Theory 44(3):580–590

Stefanini C, Orofino S, Manfredi L, Mintchev S, Marrazza S, Assaf T, Capantini L, Sinibaldi E, Grillner S, Wallén P, Dario P (2012) A novel autonomous, bioinspired swimming robot developed by neuroscientists and bioengineers. Bioinspir Biomim 7(2):1748–3190

Stefanini C, Mintchev S, Dario P (2011) Permanent magnet actuator for adaptive actuation. US Patent US20110266904, 2011

Webb B (2000) What does robotics offer animal behaviour? Animal Behav 60:545–558

Webb B, Consi T (2001) Biorobotics: methods and applications. AAAI/MIT Press, Cambridge, MA

Webb B (2001) Can robots make good models of biological behaviour? Behav Brain Sci 24(6):1033–1050

Webb B (2008) Using robots to understand animal behaviour. Adv Study Behav 38:1–58